Hybridized plasmon modes in a system of metal thin film–nanodisk array

B. C. Yildiz (iD), M. Habib (iD), A. R. Rashed (iD), and H. Caglayan (iD)

View Online   Export Citation   CrossMark

Hybridized plasmon modes in a system of metal thin film–nanodisk array

View Online   Export Citation   CrossMark

B. C. Yildiz, M. Habib, A. R. Rashed, and H. Caglayan[a]

AFFILIATIONS

Faculty of Engineering and Natural Sciences, Photonics Laboratory, Tampere University, 33720 Tampere, Finland

[a]Electronic mail: humeyra.caglayan@tuni.fi

ABSTRACT

Controlling the hybridization is a very powerful tool to manipulate the modes in a single nanostructure. We investigate the hybridization between localized and propagating surface plasmons in a nanostructure system where a thin metal layer strongly interacts with a nanodisk array. Hybrid plasmon resonances are observed in the reflection spectra obtained from finite-difference time domain simulations and experimental measurements in the visible-near-infrared region. We demonstrate how the geometrical parameters of the nanostructure can be utilized to bring these plasmon modes in the strong coupling regime. The hybrid plasmon modes exhibit anticrossing with a Rabi splitting of ~0.1 eV, which is the signature of strong coupling. Near-field profiles of the hybrid modes exhibit a mixture of localized and propagating plasmon characteristics, with propagating modes excited on both sides of the metal film. Our design promises richer implementations in light manipulation towards novel photonic applications compared to the systems with thick metal films.

I. INTRODUCTION

Plasmon hybridization theory[1] was developed to understand the response of complex plasmonic systems of arbitrary shapes, where multiple plasmon modes are supported. It describes the complex system as the interaction or "hybridization" of elementary plasmons supported by nanostructures. Hybridization of the elementary plasmon modes leads to a split in the plasmon resonance of the complex system into two energy levels: a bonding mode with a low-energy level and an antibonding mode with a higher energy level. The terms bonding and antibonding are similar to the molecular orbital theory, as the plasmon hybridization model is developed as the nanoscale electromagnetic analog of how atomic orbitals interact to form molecular orbitals in the electronic structure theory. This model has been successfully applied to a variety of plasmonic structures, such as metallic nanodimers,[2] metallic nanoshells,[3–5] metallic nanotubes,[6–8] and metallic nanoparticles near metal films.[9,10] In these studies, hybridization between different localized surface plasmons (LSPs) has been investigated. It has also been of interest how LSPs and propagating counterpart of LSPs, surface plasmon polaritons (SPPs), interact with each other.[11–16] Cesario *et al.*[17] observed the extinction of a hybrid nanostructure where a 2D nanoparticle array interacts with a thin metal film, displaying multiple resonances. This observation has been attributed to

the plasmon hybridization between localized and propagating modes, with the assumption that the propagating plasmons are present only on one of the interfaces. In another work, it has been observed that triangular-shaped silver nanoparticles and a thin silver film display strong coupling, where the propagating plasmons are excited in one of the surfaces by Kretschmann configuration.[18] The hybridization between LSP and guided modes on a thick metal film based on band diagrams[19] and the near-field spectra has also been reported.[20] Alrasheed and Di[21] theoretically presented a strong field enhancement as a result of hybridization between the magnetic plasmon resonance and propagating surface plasmons. Strong coupling between propagating plasmons and localized plasmons supported by L-shaped metal nanostructures has been demonstrated numerically.[22] In these studies, the metal film supporting the SPPs is much thicker than the skin depth, and, therefore, the propagating plasmons are excited only on one of the metal-dielectric interfaces. However, the systems with thin metal layers allow the excitation of SPPs on both top and bottom interfaces, which provides more flexible control on the hybridization, as these modes can be easily tuned by the environment. Besides, allowing near-field enhancement on both interfaces, hybrid systems of thin metal films would provide potentially richer implementations in light manipulation, compared to the systems with thick metal films, particularly in surface

plasmon-enhanced fluorescence spectroscopy,[23] and plasmon-mediated energy transfer systems.[24]

In this paper, we experimentally and theoretically demonstrate the hybridization between a continuous thin gold film deposited on a glass substrate and a periodic gold nanodisk (ND) array that is separated from the gold film by an oxide spacer layer, in the visible-near-infrared (NIR) region. Furthermore, we analyze the nature of the hybrid modes, calculate the coupling energy, and present how the coupling between the NDs and the thin metal layer is modified by the ND size and array periodicity.

II. ELEMENTARY PLASMON RESONANCES

The studied system (shown in Fig. 1) supports the elementary plasmon modes of its components: an ND array and a thin metal film. The ND array supports a single localized resonance (LSP mode). The continuous metal film supports SPP modes that can be excited by the periodicity of the ND array as long as the ND array and the thin metal film interact with each other.

To determine the elementary LSP modes, we perform finite-difference time domain (FDTD)[25] simulations using Lumerical FDTD Solutions. We calculate the scattering cross section of a periodic ND array on 50 nm of the Al_2O_3 (oxide) layer, on a glass substrate, without the thin metal layer. The thickness of the gold NDs is 70 nm. The refractive indices of the glass and oxide materials are set constant to $n = 1.45$ and $n = 1.65$, respectively. We use the tabulated experimental data provided by Johnson and Christy[26] to simulate the electric permittivity of gold. The boundary conditions are periodic along the directions parallel to the plane wave source injection (z axis) and perfectly matched layers (PML) in the propagation direction. We note that by considering the scattering cross section of an ND array, but not an isolated ND, we encounter any possible interaction among the NDs in determining the elementary LSP mode. In fact, a full treatment of the plasmon response of the ND array would encounter the lattice effect, known as surface lattice resonance (SLR),[27,28] arising out of the coupling between the plasmon resonance of the individual NDs and diffracted waves due to the lattice geometry. Since we focus on the hybridization phenomenon, in order to keep the model simple, we consider the plasmon response of the ND array as an LSP resonance, rather than an SLR, relying on the fact that the plasmon resonance is dominantly determined by the ND size, but not by the periodicity. The resonances of the ND arrays of fixed periodicity, $p = 460$ nm, for ranging values of the ND diameter, d, from 100 nm to 180 nm,
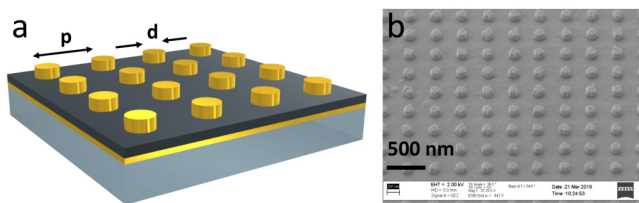

FIG. 1. (a) Schematic of the hybrid nanostructure, showing the periodicity p and nanodisk diameter d. (b) SEM image taken from the sample with $p = 460$ nm and $d = 180$ nm.
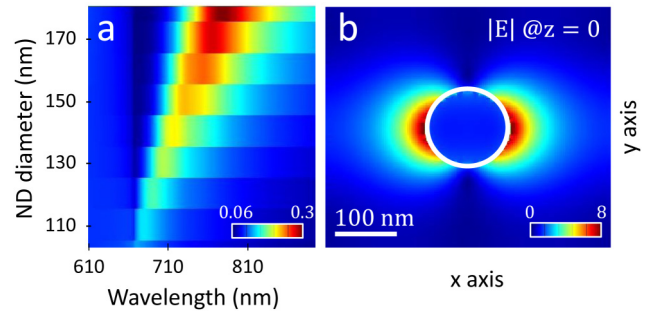

FIG. 2. (a) Localized plasmon modes of the ND arrays for fixed periodicity, $p = 460$ nm, and varying ND diameters, $d = 100–180$ nm. The color bar shows the scattering cross section in units of μm^2. (b) On-resonance (700 nm) field profile at $z = 0$ plane for $p = 460$ nm and $d = 130$ nm. The color bar shows the electric field enhancement.

with steps of 10 nm are shown in Fig. 2(a). This is a typical localized plasmon resonance resulted from the dipolar charge alignments on the NDs [Fig. 2(b)] in response to the incident field and determined fundamentally by the size and material of the ND as well as the environment.[29] We observe that the elementary LSP resonances of the system vary between 670 and 780 nm, almost linearly with the ND size.

Next, we obtain the elementary SPP modes of the system. These SPP modes are supported by the continuous thin gold layer and depend certainly on the surrounding media. The SPP modes are calculated for the multilayer structure with semi-infinite layers of air (region I) on the top and glass (region IV) at the bottom and two finite-thickness layers in between; an oxide layer with thickness $a = 50$ nm (region II); and a gold layer with thickness $b = 30$ nm (region III). In such a system, each single metal-dielectric interface can sustain bound SPPs. If the separation between adjacent interfaces is small, i.e., the metal thickness is comparable to the skin depth (~ 25 nm), the interactions between SPPs along each of the interfaces provide coupled SPP modes. To obtain these modes, we first write the E_x and H_y fields in each of the four regions. The solution of the wave equation, together with the continuity of E_x and H_y fields at the three boundaries, gives the analytical implicit dispersion relation. Hence, the propagation constant of the SPP, β, is expressed as follows:

$$\frac{k_3}{\epsilon_3}\frac{\frac{k_3/\epsilon_3+k_4/\epsilon_4}{k_3/\epsilon_3-k_4/\epsilon_4}e^{2k_3b}-1}{\frac{k_3/\epsilon_3+k_4/\epsilon_4}{k_3/\epsilon_3-k_4/\epsilon_4}e^{2k_3b}+1} = \frac{k_2}{\epsilon_2}\frac{\frac{k_1/\epsilon_1-k_2/\epsilon_2}{k_1/\epsilon_1+k_2/\epsilon_2}e^{-2k_2a}-1}{\frac{k_1/\epsilon_1-k_2/\epsilon_2}{k_1/\epsilon_1+k_2/\epsilon_2}e^{-2k_2a+1}}, \quad (1)$$

where $a(b)$ is the thickness of the region II (III) and $k_i^2 = \beta^2 - \epsilon_i k_0^2$ is the component of the wave vector perpendicular to the interface associated with each of the regions ($i = 1, 2, 3, 4$), with k_0 being the magnitude of the vacuum wavevector and ϵ_i the electric permittivity. We numerically solve this equation for varying values of the oxide thickness, a (not shown), and the metal thickness, b (Fig. 3).

Although it is not presented here, based on these calculations, we observe that for small values of the oxide thickness (10–30 nm),
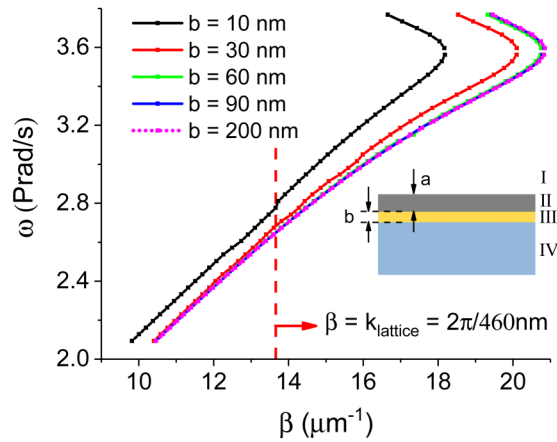
FIG. 3. SPP dispersion relation for fixed thickness of the oxide layer (region II), $a = 50$ nm, and different thicknesses of the metal layer (region III), b. In this work, b is 30 nm, which is shown by the red curve. The red perpendicular dashed line shows the $\beta = k_{lattice}$ line, where the SPP mode can be excited for a periodic structure of periodicity, $p = 460$ nm.

the dispersion curves are very similar to the dispersion of the air-gold-glass model and not affected from the existence of the oxide layer. On the other hand, for moderate values (40–80 nm), the dispersion curves lie between the ones calculated from the air-gold-glass model and oxide-gold-glass model. Finally, when a is equal or larger than ∼100 nm, the system behaves as an oxide-gold-glass structure, completely ignoring the presence of air on the top. In this work, the oxide layer is 50 nm; hence, the complete model (air-oxide-gold-glass) is required. The oxide layer thickness is set by considering the maximum interaction regime between the LSP and SPP modes.

Figure 3 shows the dispersion curves of five different metal thicknesses, b, where the oxide layer thickness is fixed to $a = 50$ nm. We observe that the dispersion curves for metal thicknesses comparable (30 nm) with, and less (10 nm) than the skin depth, are distinct from the ones for larger thicknesses, where SPPs propagate along the single interface. In this work, the metal thickness, b, is 30 nm. Therefore, SPP propagation is expected to emerge at each of the interfaces. To excite an SPP mode, the momentum of the SPP wave is required to be matched either with one of the x component of the incident light or any additional momentum contribution. In the studied case, the light is normally incident, and hence, the only way to excite the SPP modes would be using the periodicity of the ND array as gratings. Therefore, the elementary SPP resonances of the system are found at the intersections of the red dispersion curve with $\beta = k_{lattice} (= 2\pi/p)$ lines, for any periodicity, p, in Fig. 3. We find that the elementary SPP resonances of the system vary between 620 and 820 nm, almost linearly with p, varying in the range of 400–540 nm.

III. HYBRIDIZED PLASMON RESONANCES

The hybridized plasmon modes of the overall system are demonstrated experimentally by the reflection spectra, where two

pronounced resonances are observed. We fabricate the nanostructure shown in Fig. 1, for varying values of d and p. The 30 nm metal layer is deposited on a glass substrate, using an electron beam evaporator, and the 50 nm oxide layer is deposited using the atomic layer deposition technique. The electron beam lithography technique is used to fabricate the array of NDs on top of the oxide layer. The thickness of the NDs is 70 nm. The SEM image of the fabricated sample with $p = 460$ nm and $d = 180$ nm is presented in Fig. 1(b). Reflection measurements are performed by a confocal microscope, where the incident light is focused on the nanostructure by a $50\times$ objective. The reflected light is collected by a CCD spectrometer. The acquired signal is normalized to the reflected beam from a perfect mirror.

Experimental reflection spectra are shown by solid lines in Fig. 4. In Fig. 4(a), we present two modes for a fixed periodicity of $p = 460$ nm and increasing ND diameter, d, from 160 nm to 180 nm. In Fig. 4(b), we observe the reflection spectra for a fixed ND diameter of $d = 140$ nm and increasing periodicity from 400 nm to 440 nm. We refer the two resonances as the first hybrid resonance, $\lambda_{HYB}^{(+)}$ (short wavelength or high energy), and the second hybrid resonance, $\lambda_{HYB}^{(-)}$ (long wavelength or low energy), for the rest of the paper. The dashed lines are obtained from FDTD simulations, which agree with the experimental data. It is notable that for the case of fixed p, changing d does not alter the first hybrid resonance but shifts the second one to the right [Fig. 4(a)]. On the other hand, the case of fixed d and changing p exhibits a larger shift in the first hybrid resonance than the one in the second hybrid resonance [Fig. 4(b)].

To understand the hybridization between plasmon modes comprehensively, we study the system more thoroughly by observing the resonances for a wide range of periodicity and ND size and
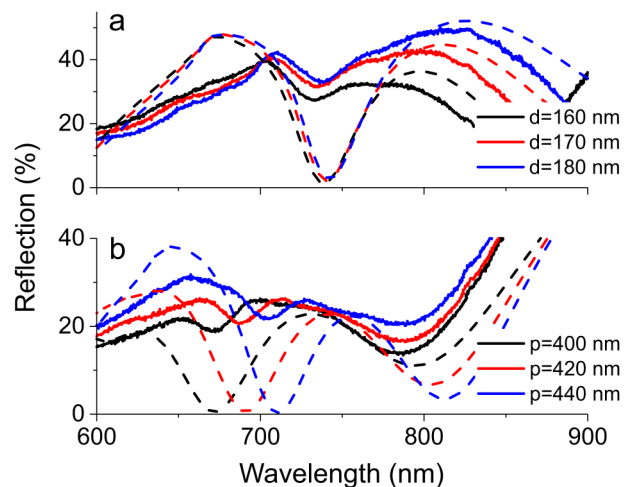

FIG. 4. Reflection spectra of the overall system for (a) fixed periodicity, $p = 460$ nm, and changing ND diameter, $d = 160, 170,$ and 180 nm and for (b) fixed $d = 140$ nm and changing $p = 400, 420,$ and 440 nm. Solid lines are obtained from reflection measurements, and dashed lines are obtained from FDTD simulations.

compare these with the elementary plasmon resonances. Figure 5 shows both the hybrid and the elementary plasmon resonances of the system for the fixed periodicity, $p = 460$ nm, and varying ND diameters in panel a and for the fixed ND diameter, $d = 130$ nm, and varying periodicities in panel b. The reflection spectra display two distinct resonances as stated earlier. The first hybrid resonance (pink lines) and the second hybrid resonance (blue lines) for changing periodicities and diameters are obtained from FDTD simulations. Black lines are the elementary LSP resonance that is obtained from the scattering cross-section simulations [as shown in Fig. 2(a)]. Red lines are the elementary SPP resonance that is calculated from the dispersion relation of the three-interface model, shown in Fig. 3. We observe both for periodicity and ND diameter sweeps that the first and the second resonances of the overall system are very close to the elementary resonance lines, except at and around the intersections of these lines. For the cases away from the anticrossing point, the two resonances are associated with the elementary LSP and SPP modes. They are weakly hybridized modes, dominantly carrying characteristics of one of the elementary modes. At the intersection, which corresponds to $p = 460$ nm and $d = 130$ nm, the first and second resonances, 675 nm and 760 nm, respectively, are split from the elementary LSP and SPP resonances, both of which are originally at ~700 nm. The anticrossing behavior shows that the ND array and the continuous thin gold film are in the strong coupling regime.[30] In this regime, Rabi splitting of the elementary plasmon mode energies of the same amount arises because of two hybridized modes with different local field distributions. At the anticrossing point, the resonances are no longer associated with the elementary LSP or SPP modes; instead, they are strongly hybridized plasmon modes, carrying characteristics of both the plasmon modes. To demonstrate this, we obtain the
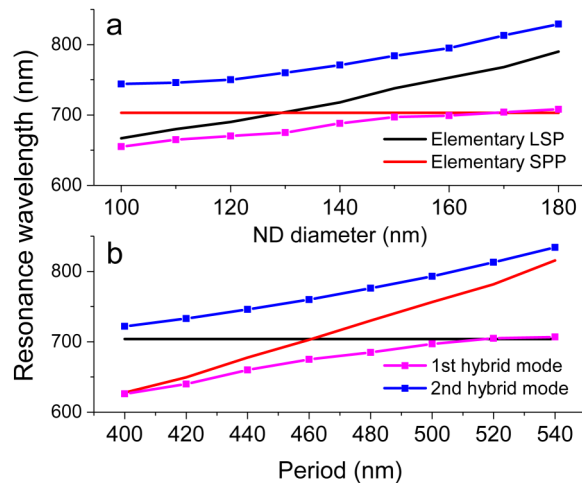
on-resonance field and phase profiles of the hybrid modes at the anticrossing point. Figures 6(a)–6(d) show the magnitude of the electric and magnetic fields, and Figs. 6(e)–6(h) show the phase profiles of the field components at the resonance wavelengths ($\lambda_{HYB}^{(\pm)}$) of the system of periodicity 460 nm and ND diameter 130 nm. We present the reflection, transmission, and absorption spectra of the hybrid nanostructure with the same geometrical properties in Fig. 6(i). We observe characteristics of both LSP and SPP modes in both field profiles. At $\lambda_{HYB}^{(+)} = 675$ nm, we observe a
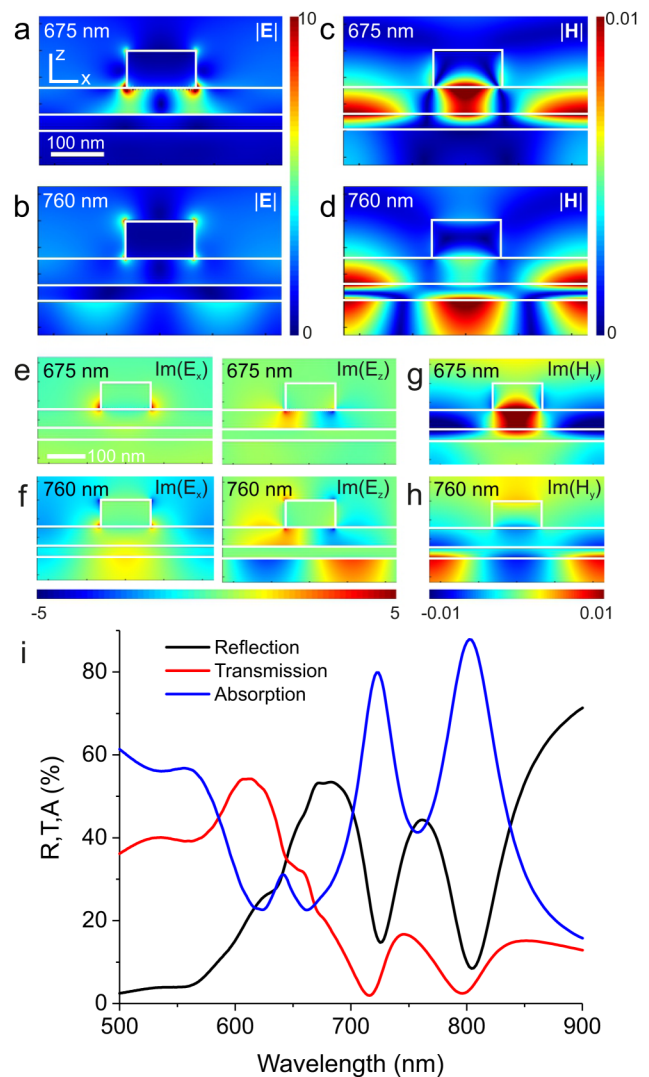

FIG. 6. Normalized field (a)–(d) and phase profiles (e)–(h) at the $y = 0$ plane, at the first (675 nm) and second (760 nm) resonances of the reflection spectrum (indicated at the upper left corner of each profile), simulated for the anticrossing point where $p = 460$ nm and $d = 130$ nm. White borders indicate the borders of the nanostructure system. (i) Reflection, transmission, and absorption spectrum, calculated at the anticrossing point.

FIG. 5. Elementary and hybrid plasmon modes for (a) varying ND diameter, d, with the fixed periodicity $p = 460$ nm and for (b) varying p, with the fixed $d = 130$ nm. Red solid lines: SPP resonance calculated from the dispersion relation given by Eq. (1). Black solid lines: Scattering cross-sectional peak of the ND array. Pink and blue lines: the first and the second resonances of the reflection spectrum.

mixture of a dipolar localized mode and a propagating mode along the gold-oxide interface. On the other hand, at $\lambda_{HYB}^{(-)}$, which is 760 nm, we observe a mixture of a quadrupole localized mode and a propagating mode along the glass-gold interface, which would not be possible with a thick metal layer. This is the key outcome of this work. Contrarily to the case of a hybrid system where a thick metal layer is employed, rather than a thin one, the proposed system provides field confinement on both of the metal surfaces. Since the resonances of this system are hybridized modes of plasmon fields, they could be flexibly tuned by the geometrical parameters: periodicity, ND diameter, and layer thicknesses, as well as the material types. As a comparison with other platforms where the propagating modes are generated without hybridization, tunability is limited with the material type in prism-coupled configurations and with environment and periodicity in grating-coupled configurations.

IV. RABI SPLITTING OF THE COUPLED MODES

Finally, we complete the hybridization picture by calculating, theoretically, the energies of the hybrid modes. We examine the coupling between two plasmonic modes, which can be considered as two coupled harmonic oscillators. We use a simple model of two coupled undamped harmonic oscillators to calculate the individual LSP and SPP resonances by using the Rabi split energy found in Sec. III. When the coupling strength exceeds the decoherence rate of the uncoupled oscillators, strong coupling occurs, and the energy exchange between the oscillators becomes the dominant

relaxation channel. In this regime, the energy levels of hybrid modes can be significantly altered, in which Rabi splitting is observed as a distinguishable characteristic of the optical response.[11,31–34] The hybrid modes resulting from the strong interaction of such two coupled oscillators are given by the expression

$$\epsilon_{HYB}^{(\pm)} = \frac{1}{2}(\epsilon_{LSP} + \epsilon_{SPP}) \pm \frac{1}{2}\sqrt{(\epsilon_{LSP} - \epsilon_{SPP})^2 + 4|\Delta|^2}, \quad (2)$$

where $\epsilon_{LSP(SPP)}$ is the energy of the uncoupled LSP (SPP) mode, in units of electron volt, that is calculated using $\epsilon_{LSP(SPP)} = hc/\lambda_{LSP(SPP)}$, with c being the speed of light in vacuum and h the Planck constant. Δ is the energy shift term (Rabi splitting energy = 2Δ). The half of the split between the first and the second resonances of the reflection spectrum at the anticrossing point can be considered as the shift term in this formula, which is found as $\Delta = 105$ meV. Using this, in Eq. (2), we calculate the theoretical low- and high-energy modes at the anticrossing point, where both of the uncoupled mode energies are the same ($\lambda_{LSP} = \lambda_{SPP} = 700$ nm). The theoretical hybrid resonance wavelengths are given in Fig. 7, together with the completed hybridization scheme of the proposed structure in the strong coupling regime. The calculated high- and low-energy modes (661 and 745 nm) are slightly different than what we obtain from the reflection spectrum (675 and 760 nm). The theoretical coupled oscillator model in the strong coupling regime reproduces the results of Sec. III.

V. CONCLUSIONS

In summary, we observe hybridization between localized and propagating plasmon modes in a coupled system of a gold nanodisk array and a continuous thin gold film. The strong coupling regime is obtained by the anticrossing behavior of hybrid plasmon resonances for varying ND diameters and structure periodicities. We observe that the energy shift is the highest at the anticrossing point, which corresponds to the same resonance wavelengths of the elementary LSP and SPP modes. The on-resonance field profiles display a mixture of LSP and SPP characteristics. The localized nature is dipolar in the first hybrid resonance, whereas it is quadrupolar in the second hybrid resonance. The propagating part of the hybrid mode is dominant along the gold-oxide interface in the first hybrid resonance and along the gold-glass interface in the second one. Such a rich-feature nanostructure follows from the control over the geometrical parameters, as we report here, and it is possible to further optimize this system by different dielectric materials. This hybrid system with two distinct resonances would be beneficial in energy transfer systems and sensing. Most importantly, allowing the excitation of SPPs at each surface, the proposed model provides flexibility in plasmon-mediated applications, where the propagating plasmons are utilized. One can benefit from the field confinement at the back side of the metal layer, in addition to the front side, in quantum emitter-metal hybrid nanostructure systems.[35] It is also possible to manipulate the energy transfer between quantum emitters and plasmon fields so that the emitters are excited at one plasmon resonance wavelength, whereas they emit at the other, in a configuration where the emitters are located on each side of the metal layer.
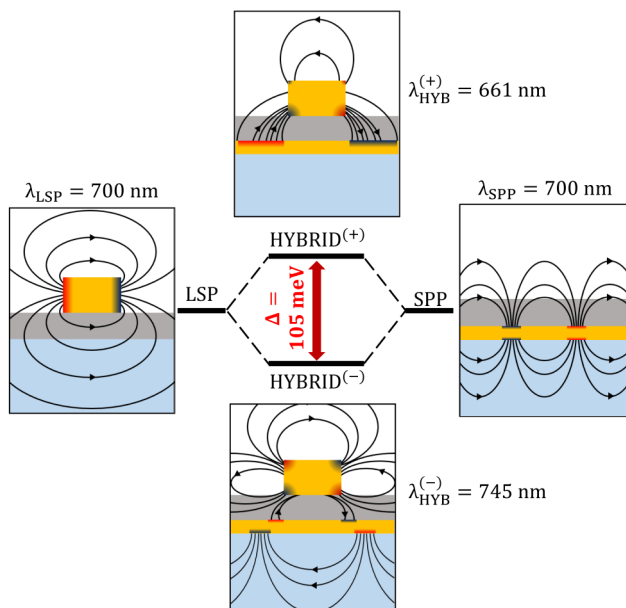
FIG. 7. Hybridization scheme. Hybrid mode resonance wavelengths are calculated using the strong interaction of two coupled oscillators, with $\Delta = 105$ meV, which is obtained from the reflection spectra.

REFERENCES

[1] E. Prodan, C. Radloff, N. J. Halas, and P. Nordlander, "A hybridization model for the plasmon response of complex nanostructures," Science **302**, 419–422 (2003).

[2] P. Nordlander, C. Oubre, E. Prodan, K. Li, and M. I. Stockman, "Plasmon hybridization in nanoparticle dimers," Nano Lett. **4**, 899–903 (2004).

[3] E. Prodan and P. Nordlander, "Plasmon hybridization in spherical nanoparticles," J. Chem. Phys. **120**, 5444–5454 (2004).

[4] C. Radloff and N. J. Halas, "Plasmonic properties of concentric nanoshells," Nano Lett. **4**, 1323–1327 (2004).

[5] D. W. Brandl, C. Oubre, and P. Nordlander, "Plasmon hybridization in nanoshell dimers," J. Chem. Phys. **123**, 024701 (2005).

[6] A. Moradi, "Plasmon hybridization in metallic nanotubes," J. Phys. Chem. Solids **69**, 2936–2938 (2008).

[7] A. Moradi, "Plasmon hybridization in metallic nanotubes with a nonconcentric core," Opt. Commun. **282**, 3368–3370 (2009).

[8] A. Moradi, "Plasmon hybridization in coated metallic nanowires," J. Opt. Soc. Am. B **29**, 625 (2012).

[9] P. Nordlander and E. Prodan, "Plasmon hybridization in nanoparticles near metallic surfaces," Nano Lett. **4**, 2209–2213 (2004).

[10] F. Le, N. Z. Lwin, N. J. Halas, and P. Nordlander, "Plasmonic interactions between a metallic nanoshell and a thin metallic film," Phys. Rev. B **76**, 165410 (2007).

[11] H. Shan, Y. Yu, X. Wang, Y. Luo, S. Zu, B. Du, T. Han, B. Li, Y. Li, J. Wu, F. Lin, K. Shi, B. K. Tay, Z. Liu, X. Zhu, and Z. Fang, "Direct observation of ultrafast plasmonic hot electron transfer in the strong coupling regime," Light Sci. Appl. **8**, 9 (2019).

[12] Q. Li, J. Gao, H. Yang, H. Liu, X. Wang, Z. Li, and X. Guo, "Tunable plasmonic absorber based on propagating and localized surface plasmons using metal-dielectric-metal structure," Plasmonics **12**, 1037–1043 (2017).

[13] C. V. Hoang, K. Hayashi, Y. Ito, N. Gorai, G. Allison, X. Shi, Q. Sun, Z. Cheng, K. Ueno, K. Goda, and H. Misawa, "Interplay of hot electrons from localized and propagating plasmons," Nat. Commun. **8**, 771 (2017).

[14] G. Lévêque and O. J. F. Martin, "Optical interactions in a plasmonic particle coupled to a metallic film," Opt. Express **14**, 9971 (2006).

[15] T. Weber, T. Kiel, S. Irsen, K. Busch, and S. Linden, "Near-field study on the transition from localized to propagating plasmons on 2D nano-triangles," Opt. Express **25**, 16947 (2017).

[16] W. Cui, W. Peng, L. Yu, X. Luo, H. Gao, S. Chu, and J.-F. Masson, "Hybrid nanodisk film for ultra-narrowband filtering, near-perfect absorption and wide range sensing," Nanomaterials **9**, 334 (2019).

[17] J. Cesario, R. Quidant, G. Badenes, and S. Enoch, "Electromagnetic coupling between a metal nanoparticle grating and a metallic surface," Opt. Lett. **30**, 3404 (2005).

[18] S. Balci, E. Karademir, and C. Kocabas, "Strong coupling between localized and propagating plasmon polaritons," Opt. Lett. **40**, 3177–3180 (2015).

[19] W. Zhou, J. Y. Suh, Y. Hua, and T. W. Odom, "Hybridization of localized and guided modes in 2D metal–insulator–metal nanocavity arrays," J. Phys. Chem. C **117**, 2541–2546 (2013).

[20] Y. Chu and K. B. Crozier, "Experimental study of the interaction between localized and propagating surface plasmons," Opt. Lett. **34**, 244 (2009).

[21] S. Alrasheed and E. Di, "Giant magnetic field enhancement in hybridized MIM structures," IEEE Photonics Technol. Lett. **29**, 2151–2154 (2017).

[22] J. Chen and J. Hu, "Strong coupling between localized and propagating surface plasmon modes in a noncentrosymmetric metallic photonic slab," J. Opt. Soc. Am. B **31**, 1600–1606 (2014).

[23] L. Touahir, A. T. A. Jenkins, R. Boukherroub, A. C. Gouget-Laemmel, J.-N. Chazalviel, J. Peretti, F. Ozanam, and S. Szunerits, "Surface plasmon-enhanced fluorescence spectroscopy on silver based SPR substrates," J. Phys. Chem. C **114**, 22582–22589 (2010).

[24] P. Andrew and W. L. Barnes, "Energy transfer across a metal film mediated by surface plasmon polaritons," Science **306**, 1002–1005 (2004).

[25] A. Taflove and S. C. Hagness, *Computational Electrodynamics: The Finite-Difference Time-Domain Method* (Artech House, 2005), p. 1006.

[26] P. B. Johnson and R. W. Christy, "Optical constants of the noble metals," Phys. Rev. B **6**, 4370–4379 (1972).

[27] V. G. Kravets, A. V. Kabashin, W. L. Barnes, and A. N. Grigorenko, "Plasmonic surface lattice resonances: A review of properties and applications," Chem. Rev. **118**, 5912–5951 (2018).

[28] D. Khlopin, F. Laux, W. P. Wardley, J. Martin, G. A. Wurtz, J. Plain, N. Bonod, A. V. Zayats, W. Dickson, and D. Gérard, "Lattice modes and plasmonic linewidth engineering in gold and aluminum nanoparticle arrays," J. Opt. Soc. Am. B **34**, 691 (2017).

[29] K. L. Kelly, E. Coronado, L. L. Zhao, and G. C. Schatz, "The optical properties of metal nanoparticles: The influence of size, shape, and dielectric environment," J. Phys. Chem. B **107**, 668–677 (2003).

[30] A. Ghoshal and P. G. Kik, "Theory and simulation of surface plasmon excitation using resonant metal nanoparticle arrays," J. Appl. Phys. **103**, 113111 (2008).

[31] M.-E. Kleemann, R. Chikkaraddy, E. M. Alexeev, D. Kos, C. Carnegie, W. Deacon, A. C. de Pury, C. Große, B. de Nijs, J. Mertens, A. I. Tartakovskii, and J. J. Baumberg, "Strong-coupling of WSe$_2$ in ultra-compact plasmonic nanocavities at room temperature," Nat. Commun. **8**, 1296 (2017).

[32] R. Thomas, A. Thomas, S. Pullanchery, L. Joseph, S. M. Somasundaran, R. S. Swathi, S. K. Gray, and K. G. Thomas, "Plexcitons: The role of oscillator strengths and spectral widths in determining strong coupling," ACS Nano **12**, 402–415 (2018).

[33] A. Konrad, A. M. Kern, M. Brecht, and A. J. Meixner, "Strong and coherent coupling of a plasmonic nanoparticle to a subwavelength Fabry–Pérot resonator," Nano Lett. **15**, 4423–4428 (2015).

[34] L. Shi, T. Hakala, H. Rekola, J.-P. Martikainen, R. Moerland, and P. Törmä, "Spatial coherence properties of organic molecules coupled to plasmonic surface lattice resonances in the weak and strong coupling regimes," Phys. Rev. Lett. **112**, 153002 (2014).

[35] P. Vasa and C. Lienau, "Strong light–matter interaction in quantum emitter/metal hybrid nanostructures," ACS Photonics **5**, 2–23 (2018).